Organic solvent reverse osmosis using CuAAC-crosslinked molecularly-mixed composite

2 membranes

3

1

4 Matthew P. Rivera^a, Nicholas C. Bruno^b, M.G. Finn^b, Ryan P. Lively*^a

5

- 6 aSchool of Chemical and Biomolecular Engineering, Georgia Institute of Technology, Atlanta, GA
- 7 bSchool of Chemistry and Biochemistry, Georgia Institute of Technology, Atlanta, GA

8

- 9 Corresponding author: Ryan P. Lively; ryan.lively@chbe.gatech.edu
- 10 Permanent address: Ford Environment Science and Technology Building, 311 Ferst Dr NW,
- 11 Atlanta, GA 30332

12

13

Abstract

14 Molecularly-mixed composite membranes (MMCMs) incorporating amorphous scrambled porous 15 organic cages (ASPOCs) are a rapidly emerging membrane class that are characterized by the 16 formation of a solid solution due to a high degree of homogeneity that is not observed in other 17 classes of polymer-particle composites. Molecular-level mixing overcomes many of the 18 performance/processing issues typically encountered with two phase composite materials. 19 However, chemical stabilization of the polymer matrix can deactivate the ASPOC cages. Here, we 20 illustrate an alternative method of crosslinking Matrimid® in MMCMs using the copper catalyzed 21 azide alkyne cycloaddition (CuAAC) click reaction. We fabricated thin film composite membranes 22 and benchmarked them in a crossflow permeation system with standard styrene oligomers 23 dissolved in a variety of organic solvents as well as an exemplar organic solvent reverse osmosis 24 separation. We found that the presence of ASPOC increased both permeance and styrene dimer 25 separation factor by up to 79% and 154%, respectively, over crosslinked Matrimid depending on 26 the solvent, although the separation factor decreased at higher ASPOC loadings. The crosslinked 27 MMCMs were challenged with a solvent-solvent separation in an organic solvent reverse osmosis 28 modality and were able to effectively purify toluene from triisopropylbenzene. This work provides 29 experimental observations needed to understand the mass transport processes occurring in 30 MMCMs and highlights their separation performance and scale-up potential.

32	Keywords
33	Molecularly mixed composite membrane; Crosslinking; Porous organic cage; Organic solven
34	reverse osmosis; Polyimide
35	
36	
37	
38	

1. Introduction

Rising energy demand and associated carbon emissions represent a significant global challenge. A key sustainability target is to decrease the energy expenditures required by industrial separation processes. Membrane-based separations are inherently energy-efficient and so offer promising ways to augment or replace certain thermal separations, potentially reducing energy requirements by up to 90%, as was demonstrated in the case of seawater reverse osmosis relative to multi-stage flash evaporation.[1] Polymeric membranes already see application in many areas such as natural gas sweetening [2], oxygen enrichment [3], and seawater reverse osmosis [4]. One area where membranes have received less commercial attention are separations in organic environments. Two important separation modalities in this area are organic solvent nanofiltration (OSN) and organic solvent reverse osmosis (OSRO). While these modalities are closely related, they have important, subtle distinctions based on the driving force for the separation, with OSN being driven by a pressure gradient across the membrane and OSRO being driven by a pressure-induced concentration gradient across the membrane.[5] Membrane-based separations in these regimes are often limited due to an inverse relationship between permeability and selectivity, which can ultimately limit product recovery and purities [6].

Microporous materials, such as zeolites and metal-organic frameworks (MOFs), offer a potential general solution to this problem, having shown both excellent permeability and selectivity for many challenging systems.[7-9] Despite excellent separation capabilities, their prohibitive cost as well as difficulties associated with fabrication into large-scale, defect-free membranes have prevented widespread implementation. Mixed matrix membranes (MMMs) combine the desirable aspects of these two classes of materials. In MMMs, a microporous material is dispersed as a filler phase throughout a polymer matrix to combine the separation capabilities of the former with the processability of the latter.[10-13]

The development of new classes of porous materials in recent years [14-16] has made available more types of fillers for use in MMMs.[17, 18] Of particular note are porous organic cages (POCs), organic macrocycle molecules that can dissolve into solvents while still maintaining distinct, self-supported cage structures with permanent porosity.[15] With self-supported porosity and an approximated molecular diameter of 1.8 nm, they are "zero-dimensional" point structures relative to the typical size of polymer chains, as opposed to other particle-like MMM fillers, which can be anywhere from tens of nanometers to hundreds of microns in size. Because of their organic

nature and their existence as single molecules instead of continuous extended structures, POCs represent promising filler phases for MMMs. The intimate interactions expected between individual cage molecules and surrounding polymer chains may potentially alleviate interfacial issues often observed with macromolecular fillers.[18] Additionally, POCs have proven adept at challenging gas separations.[19, 20] We believe that POCs provide an ideal filler phase for composite membrane materials because of their proven separation abilities and processing advantages.

In previous work attempting to form MMCMs with POCs,[21] relatively large POC crystals were observed to form upon phase inversion such that classical MMM-type membranes were formed. This ultimately led to void spaces between the two primary phases and reduced membrane selectivity. The problem of crystal formation was subsequently addressed with mixtures of POCs incorporating different linkers or functional groups, a subclass known as amorphous scrambled porous organic cages (ASPOCs).[22-24] This provides the opportunity to form molecularly mixed composite membranes (MMCMs) with the filler and continuous phases intertwined at a molecular level[21, 22, 25], giving rise to an effectively one-phase 'solid solution.'[25] Such single-phase composites should be much easier to adapt to current membrane processing technology than traditional two-phase MMMs where issues such as filler agglomeration and interfacial defects are common.[26, 27]

Polyimides are commonly used in separation applications, including in MMMs.[28, 29] To reduce plasticization or solvation by organic solvents, the polymers are often crosslinked,[30] most often with primary diamines. However, such diamines would degrade many ASPOC structures, which are held together by thermodynamically and kinetically weak imine linkages. We therefore explored the use of the copper-catalyzed azide-alkyne cycloaddition (CuAAC) click reaction as a method for crosslinking Matrimid 5218 that should leave the ASPOC fillers intact. The CuAAC reaction is often orthogonal to other chemistries used to make and modify a wide variety of polymers; its 1,4-disubstituted triazole products are highly stable towards heat, oxidation, and hydrolysis. The CuAAC reaction can be very rapid and is irreversible, making it a powerful method for post-polymerization functionalization.[31]

To test the CuAAC reaction for crosslinking Matrimid in ASPOC MMCMs, and to investigate the ability of these MCMMs to perform challenging organic solvent separations, thin-film composite membranes of Matrimid and MMCMs were prepared with suitable azide and

alkyne functionality (Figure 1). Crosslinking was performed by first introducing alkyne groups into the polymer backbone by imide ring-opening with propargyl amine prior to membrane fabrication, followed by submerging the resulting membrane in a methanolic solution of 1,10-diazidodecane and Cu(I). The effects of propargylation on the properties of the starting Matrimid polymer were investigated with dynamic light scattering (DLS) and thermogravimetric analysis (TGA), and separation performance as a function of crosslinking and ASPOC loading was determined with polystyrene standards in several solvents (including solvents that are incompatible with uncrosslinked MMCMs) and separation of toluene and triisopropylbenzene in a custom-built crossflow permeation system. From these results, we provide some insight into the underlying mechanisms of organic molecule transport through MMCMs.

2. Experimental

112 2.1 Materials

101

102

103

104

105

106

107

108

109

110

111

- 113 Matrimid 5218 was purchased from Ribelin. Commercially-available reagents were used as
- 114 received: 1,3,5-benzenetricarbaldehyde (Manchester Organics); (1R,2R)-1,2-
- 115 cyclohexanediamine, ethylenediamine, lithium nitrate, triisopropylbenzene (TIPB) and p-
- 116 xylylenediamine (Sigma Aldrich); propargylamine (Oakwood Chemical); and solvents (VWR or
- Fisher Scientific). 1,10-diazidodecane[32] and bis(triphenylphosphine) copper (I) acetate[33]
- were synthesized according to literature procedures. Polystyrene standards consisting of α-
- methylstyrene dimer, a standard mixture with an average molecular weight of 580 Da (PS 580),
- and a standard mixture with an average molecular weight of 1300 Da (PS1.3k) were obtained from
- 121 Agilent Technologies and used without further purification.

- 123 2.2 Synthesis of ASPOC
- ASPOC was synthesized using the procedure described previously.[21] 1,3,5-
- Benzenetricarbaldehyde (500 mg) was dissolved in 40 mL of anhydrous dichloromethane.
- Ethylenediamine (CC1 linker, 45 mg) and (1R,2R)-1,2-cyclohexanediamine (CC3-R linker, 87.5
- mg) were dissolved in a separate vessel with 40 mL anhydrous dichloromethane. The two solutions
- were combined and stirred at room temperature for three days. The solvent was subsequently
- removed by rotary evaporation, and the resulting yellow powder was soaked in ethyl acetate for
- one day and isolated by centrifugation. This wash was performed three times, replacing with fresh
- solvent each day. The resulting off-white powder was dried at 80 °C under vacuum overnight.

2.3 Thin-film composite (TFC) support fabrication

Matrimid was dried at 110 °C overnight. A dope of the following composition by weight percent was prepared with anhydrous solvents: Matrimid:NMP:THF:ethanol:LiNO3:deionized water = 16:69:10:3:1:1. The dope was mixed on a rolling mixer overnight and then stood upright for 12 hours to degas. In a fume hood on a dry glass plate, the dope was cast with a 10 mil casting blade, and the film was allowed to stand for 10 s before transfer to a deionized water bath. The film was solvent exchanged for approximately 20 minutes before transfer to another fresh DI water bath for 24 hours. The support was then solvent exchanged with methanol three times for several hours each. The supports were then submerged in a solution of 5%w/v (i.e., 5 g per 100 mL of solution) p-xylylenediamine in methanol to crosslink. The supports were allowed to react in the crosslinking solution for 24 hours and then were washed with methanol three times for several hours each. The supports were then solvent exchanged with hexane three times for several hours each and dried at 110 °C under vacuum overnight.

2.4 Thin-film composite topcoat dope preparation

Matrimid was dried in an oven under a vacuum at 80 °C overnight prior to dissolving in anhydrous chloroform such that the resulting dope was 1 wt% solids (i.e., Matrimid + ASPOC to be added later). An amount of propargylamine equimolar to the amount of Matrimid repeat unit was then added to the dope (i.e., 10 mg propargylamine per 100 mg Matrimid). The dope was mixed on a rolling mixer at room temperature for two days. Once the reaction was complete, the balance of ASPOC was added to create a 1 wt% solids solution. While other methods of incorporating the POC into the polymer matrix are certainly possible,[34] we confine ourselves to mixing cages into the initial dope solution.in this proof-of-concept work. This method is relatively straightforward in terms of processing and yields the type of composite membrane structure that we are aiming for. The dope was mixed for one day to dissolve the ASPOC; it was then filtered through a 0.2 micron PTFE filter to remove any remaining insoluble fractions and stored at 4 °C until immediately before use. All TFC samples were subject to the same fabrication and crosslinking procedure.

2.5 Thin-film composite fabrication

Thin-film composites were prepared with a Laurell WS-650-23B spincoater. Supports prepared previously were dried at 110 °C under vacuum overnight prior to use. Kimwipes were soaked in chloroform and then lined around the interior of the spincoater to saturate the atmosphere for about 15 minutes. The support was quickly placed on the chuck and the spincoating procedure begun. The support was spun at 500 rpm for 30 seconds, during which time ten drops (~0.5 mL) of the still chilled topcoat dope were dropped onto the support from a Pasteur pipette with one drop approximately every three seconds. The rotation was then increased to 1000 rpm for five minutes. The TFC was allowed to dry in the spin coater for ten more minutes before removal, followed by drying at 80 °C overnight. To crosslink, six TFCs were submerged in a 50 mL solution of 10 mg/mL each 1,10-diazidodecane and copper(I) triphenylphosphine acetate catalyst in methanol for two days at 35 °C. A large excess of azide with respect to alkyne incorporated into the polymer was used because crosslinking was observed to be inconsistent with equimolar amounts of diazide and substituted alkyne. Assuming that it is difficult for the large diazide molecule to penetrate into the membrane structure, an excess of diazide was employed to increase its diffusive driving force and ensure that a sufficient number of alkyne groups are addressed. We emphasize that long reaction times and large excesses of crosslinker were used to overcome transport limitations of the crosslinker diffusing throughout the membrane. Once anchored by a triazole at one end, intra- or inter-strand molecular crosslinking by the other end of the diazide should be efficient. The crosslinked TFCs were washed with methanol for several hours three times and dried at 80 °C under vacuum overnight. An illustration of the relevant chemistry and final product in the TFC fabrication procedure is shown in Figure 1. All samples are crosslinked unless otherwise noted. The membrane fabrication procedure was not changed based on the separation experiment (i.e., solute rejection or OSRO), as our focus is on proof-of-concept membrane fabrication methods.

163

164

165

166

167

168

169

170

171

172

173

174

175

176

177

178

179

180

181

182

183

184

185

Figure 1: Schematic for thin film composite fabrication. Note that the relative sizes of the cages and polymer chains are not to scale. 1. The polymer is chemically functionalized with alkyne moieities. 2. The ASPOC is added into the polymer solution and the thin film composite is spuncoat onto a polyimide support. 3. The

2.6 Dense film preparation

membrane is crosslinked via the CuAAC reaction

Dense membrane samples were prepared by dropping a small amount of the topcoat dope onto a Teflon petri dish and allowing the solvent to evaporate at room temperature. The dense sample was then subjected to the same crosslinking conditions as the thin-film composites.

2.7 Fourier transform infrared spectroscopy (FTIR)/Raman spectroscopy

FTIR of dense films was performed on a Nicolet iS50 equipped with an iS50 ATR module. Samples were analyzed with 128 scans at a resolution of 4 cm⁻¹. Raman mapping of Matrimid membranes was conducted on a Renishaw Raman Spectrometer Vis/near-IRequipped with an optical microscope. A 785 nm laser was used as the incident. Raman spectra were taken over amembrane area of 200 × 100 μm with a resolution of 1 μm. The ASPOC molecules have characteristic shifts at 1785 cm⁻¹, 1678 cm⁻¹, 1621 cm⁻¹, and 1378 cm⁻¹. The intensity of the 1378 cm⁻¹ was used because it provided the clearest contrast from the baseline Matrimid spectrum and was overlayed on the optical image of the membrane surface.

- 2.8 Dynamic light scattering (DLS)/Thermogravimetric analysis (TGA)
- Particle size distributions of Matrimid made from dope solutions with an increasing amount of propargylamine were measured with a Wyatt DynaPro NanoStar with a 660 nm laser and solutions of 0.5 mg/mL. Samples were prepared by dissolving 100 mg of neat Matrimid in 20 mL chloroform. Propargylamine was added on a mol% basis relative to the moles of Matrimid repeat units. The dope solution was mixed under a heat lamp for two days to achieve full conversion. The resulting dope was dropped onto a Teflon petri dish and allowed to dry. The solid polymer was then washed with methanol three times (one day each), dried at 100 °C overnight, and redissolved in chloroform for DLS measurements. Thermal stability of solid samples was investigated on a TA Instruments O500 in an air atmosphere (90 mL/min) and a 10 °C/min ramp to 900 °C.

- 2.9 Scanning Electron Microscopy (SEM)
- SEM was performed on a Hitachi SU8010. Cross-sections of membranes were prepared by cryo-fracturing. A small portion of the membrane was soaked in hexane for approximately 15 min then submerged in liquid nitrogen for 5-10 minutes. The membrane portion was broken in two, and the broken edge was placed facing upward on the sample stub. Samples were sputtered with gold using a Quorum Q-150T ES prior to imaging. Images were taken at a working voltage of 5 kV and a current of 10 mA.

- 230 2.10 Liquid permeation testing
- Permeances of the TFCs in tetrahydrofuran (THF), acetonitrile, methanol, ethanol, toluene, and heptane were measured in a custom-built crossflow permeation system with an effective

membrane area of 11.34 cm², described previously and shown in Figure S1.[21] We note that the ASPOCs used in this study are insoluble in all of the solvents tested such that any leaching of the

cages of into the solvent solution will almost certainly be negligible. Solvent flux (J_i) was

236 measured by permeate mass as follows:

235

257

258

259

260

$$237 J_i = \frac{\frac{m_i}{\rho_i}}{\frac{1}{A \cdot t}} (1)$$

- Where m is mass of permeate, ρ is the solvent density, A is the membrane available mass transfer
- surface area, and t is time. Hydraulic permeance was calculated as:

$$240 \qquad \frac{\mathbb{P}_i^H}{\ell} = \frac{J_i}{\Delta p} \tag{2}$$

Where \mathbb{P}_i^{H}/ℓ is the permeance in (L m⁻² h⁻¹ bar⁻¹), and Δp is the hydraulic pressure difference across the membrane. All experiments were performed at a pressure of 30 bar and a feed flow rate of 10 mL/min. Stage cuts varied based on the solvent used but were typically between 1-8% and

244 were intentionally kept low to reduce the effects of concentration polarization. Solute rejections in

245 each of the six solvents listed above was measured using polystyrene oligomer standards from

246 Agilent Technologies. Specifically, 0.05 g/L of α-methylstyrene dimer, 0.5 g/L of PS580, and 0.5

247 g/L of PS1.3k were dissolved in each solvent. The permeate composition was analyzed on an

248 Agilent HPLC system with a UV/Vis detector set at wavelength 264 nm. A reverse-phase column

(C18-300, 250X4.6 mm) was used with a mobile phase flow rate of 0.5 mL/min. The mobile phase

consisted of 35 vol% analytical grade water and 65 vol% analytical grade THF, each with 0.1 vol%

trifluoroacetic acid. The procedure was run for 30 min at room temp. All solvents were evaporated,

and any remaining PS oligomers were redissolved in ethanol prior to HPLC analysis. From this

data, molecular weight cut-off (MWCO) curves and the separation factor of the dimer were

254 calculated according to equations 3 and 4, respectively

$$255 R_i(\%) = \left(1 - \frac{c_{i,permeate}}{c_{i,feed}}\right) * 100 (3)$$

$$256 SF = \frac{\left(\frac{C_{dimer}}{C_{solvent}}\right)_{feed}}{\left(\frac{C_{dimer}}{C_{solvent}}\right)_{permeate}} (4)$$

Where *i* refers to a PS oligomer of a specific molecular weight. The MWCO was taken to be the minimum oligomer molecular weight for which rejection exceeded 90%. All experiments were performed in triplicate, involving three supports made as described in Section 2.3 and three separate TFCs made from the same dope solution via spin coating as described in Section 2.5.

Each membrane was tested, and the average permeance and rejection/separation factor were reported with standard deviation. Organic solvent reverse osmosis (OSRO) performance was assessed with a feed mixture of 95:5 mol% toluene:triisopropylbenzene under the same conditions as the polystyrene experiments. Permeate composition was determined on an Agilent 7890B gas chromatograph. The osmotic pressure of this mixture is ~12 bar.

2.11 Reproducibility

261

262

263

264

265

266

267

268

269

270

271

272

273

274

275

276

277

278

279

280

281

282

283

The membranes used for solute rejection and OSRO measurements were made via the spincoating process discussed in sections 2.3-2.5, using the same topcoat dope solution batch for each different ASPOC loading, coated onto separate support membranes. All permeation results are reported as the average of three successful experiments performed on different TFC membranes, with error estimated by range of the maximum and minimum values measured. Approximately 50% of the membranes made were considered to be defective, based on dramatically reduced dimer/solvent separation factors, high permeances, and poorer oligomer rejection performance. Spin coating involves complex sub-micron fluid film dynamics, and so this level of variability is to be expected. Permeation experiments were performed in a random order of solvents for each set of membranes. Some membranes failed before all solvent mixtures could be tested on them, likely due to excessive mechanical stress from repeated pressurization/depressurization (and therefore swelling/deswelling) cycles required to adequately exchange solvents in the crossflow system. In this case, failed membranes were swapped out for freshly fabricated membranes so that three data points were still obtained. All permeation measurements were performed over two days with measurements being taken each day. Measurements were found to be consistent across the time period supporting that all measurements were taken at steady-state operation. We have not studied the aging behavior of these membranes in this work.

284285

286

288

289

290

291

3. Results and Discussion

287 3.1 ASPOC Characterization

The desymmetrized ASPOC mixture incorporating ethylenediamine (CC1) and (1R,2R)-1,2-cyclohexanediamine (CC3)) was prepared and characterized by NMR (Figure S2a) as reported previously.[21] Its nitrogen isotherm measured at 77 K (Figure S2b) showed Type II isotherm features, which means a sharp initial uptake followed by low slope at intermediate relative pressure

and a steeper slope at higher relative pressures. Type II isotherms typically correspond to solids with a distribution of pore sizes.[35, 36] Here, the micropore size distribution (with a pore window diameter of 6 Å and internal pore diameter of ~7.2 Å) is expected to be relatively constant because the different ASPOC cages are quite similar in size.[24] We therefore suggest that the apparent distribution of pore sizes is actually a distribution of random, irregular void spaces between cage molecules due to inefficient packing, an idea which is supported by the observation of an isotherm hysteresis that is characteristic of the condensation of liquids in mesopores.

The BET surface area was measured to be 130 m²/g, compared to previously reported surface areas of 624 m²/g for pure CC3 and 0 for CC1 (apparently non-porous due to a lack of interconnectivity between individual cages).[15] However, BET surface area of ASPOC molecules can vary with differences in sample preparation, ranging from very high (818 m²/g) due presumably to inefficient molecular packing[24] to values lower for a mixture (CC3 and CC1) than for a homogeneous (CC3) amorphous composition.[22] Thus, we caution that the measured surface area of POC and ASPOC materials is highly dependent on long-range order, or lack thereof, in the sample due to the potential creation of microporous cavities between individual cage molecules. The ASPOC samples prepared here apparently possess low "extra-cage" adsorption capacity; however, permeation testing of composite membranes described below supports the existence of significant intrinsic cage porosity.

3.2 Effect of alkyne functionalization on Matrimid

Matrimid samples heated with different amounts of propargylamine were characterized by dynamic light scattering, as shown in Figure 2a. Average particle radius was found to decrease from approximately 1350 nm for neat Matrimid to approximately 150 nm for material treated with 50 mol% amine. Continuous membrane samples treated with more than 25 mol% propargylamine were rendered highly fragile, presumably because of increased chain mobility induced by imide ring opening and perhaps small amounts of chain scission by transamination at ring-opened sites. At the low concentrations used for DLS (5 mg/mL), the increased flexibility from the imide ring opening may have caused a high degree of intra-, as opposed to inter-, chain interaction that caused the individual chains to condense into smaller particles. For the Matrimid used in this study, it appears that the apparent particle size reducing effect of this increased intra-chain interaction has an asymptote of ~100 nm. Thermogravimetric analysis (Figure 2b) showed that neat Matrimid

exhibited three major decomposition peaks at 551, 625, and 677 °C, with the most significant decomposition occurring at 677 °C. The use of increasing amounts of propargyl amine shifted the major decomposition to somewhat lower temperature, with only one major decomposition at 612 °C observed for the 100% amine added sample. These results show that even a small amount of imide ring-opening has substantial effects on Matrimid properties, and suggests that crosslinking be explored with relatively few such connecting points. A highly reactive crosslinking reaction is therefore an asset at low functional-group densities.

Covalent crosslinking of propargylated Matrimid with the flexible diazide was verified by FTIR (Figure 3). Thus, the alkyne stretching vibration at 2093 cm⁻¹ was introduced upon reaction with propargylamine, and disappeared completely upon CuAAC reaction, suggesting at least 95% conversion to the corresponding triazole. No significant changes were observed in other regions of the infrared spectrum throughout the crosslinking process, suggesting that the click reaction retained its well-known specificity.

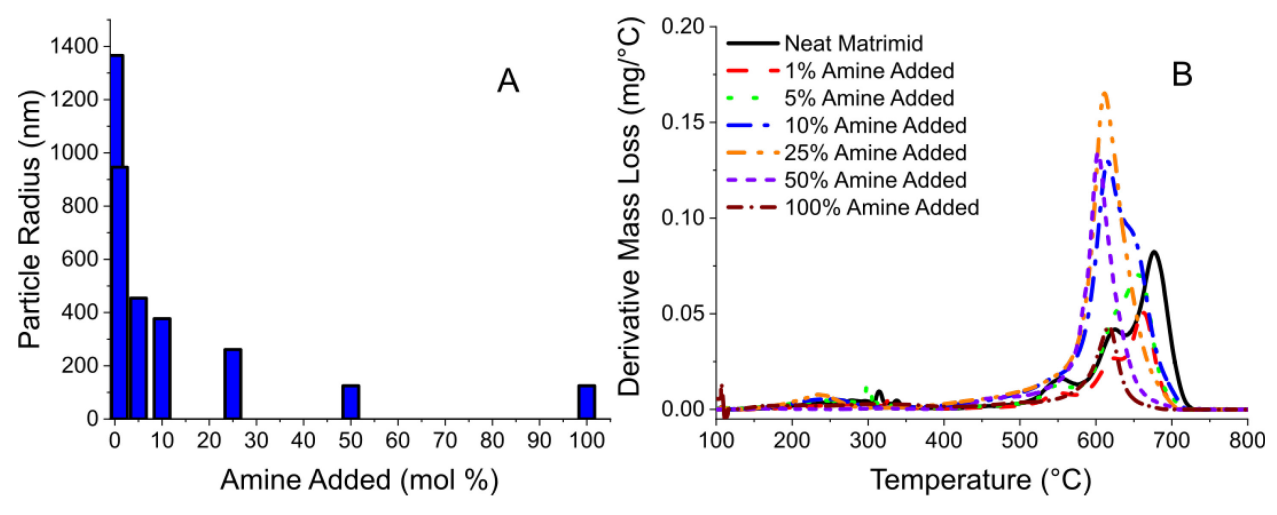


Figure 2: Effect of alkyne functionalization on Matrimid polymer backbone. (A) Most frequent particle size of Matrimid from solutions mixed with increasing amounts of propargylamine. The mol % added refers to the amount of propargylamine added to the solution relative to the amount of Matrimid repeat units. Full particle size distributions of each sample can be found in Figure S3. All samples also appeared to show a cluster between 2 and 3 nm, perhaps due to trace amounts of monomer. (B) Derivative mass loss of Matrimid samples with respect to temperature to clarify the onsets of major decompositions.

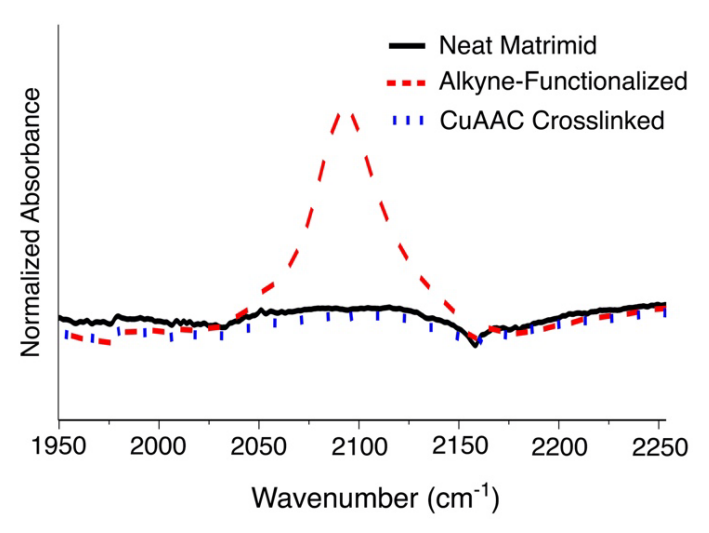


Figure 3: FTIR spectra of neat Matrimid (black), Matrimid functionalized with 100 mol% propargylamine (red), and CuAAC-crosslinked Matrimid (blue) from 1950 cm⁻¹ to 2250 cm⁻¹. The full spectra can be found in Figure S4. The absorbance of the samples is normalized by the thickness of the films on which the spectra were taken.

3.3 Thin Film Composite Structure

345346

347

348

349

350

351

352

353

354

355

356

357

358

359

360

361

362

363

364

365

366

367

368

A series of TFC samples were fabricated and crosslinked incorporating different amounts of ASPOC. Cross-sectional SEM images showed a uniform topcoat layer approximately 400 nm thick on each TFC for pure Matrimid and the 2.6 vol% ASPOC samples (Figure 4a-d). We also noted good adhesion between the topcoat and support in these materials. Although the topcoat is somewhat thicker than what is seen in many TFC examples in the literature, we were able to achieve high permeances, as discussed below. We also note that no attempt was made to optimize topcoat thickness. When the ASPOC loading was increased to 5.7 vol%, the topcoat became noticeably thicker and was not as well adhered (Figure 4e-f). With even more ASPOC (9.4 vol%), the topcoat was further increased in thickness and appeared to have partially penetrated into the support (Figure 4g-h). While topcoat thickness can be influenced by a complex interplay of factors including dope viscosity, interaction with support, and spin coating atmosphere, ASPOC loading appears to make a significant impact. However, at all loadings, the topcoat appears uniform with no significant agglomerates, supporting previous work in which the molecular dispersion of CC3derived ASPOCs in Matrimid was suggested.[21] Molecular level mixing of the ASPOCs in the crosslinked membranes was interrogated with Raman spectral surface mapping of the 2.6 vol% loading membrane at the cage characteristic peak of 1378 cm⁻¹, shown in Figure S5. A low but fairly uniform concentration of the cages is observed across the scanned space supporting the

dispersion of the cages. In previous work, molecular interaction of the cages was confirmed via a shift in the glass transition temperature with dynamic scanning calorimetry; however, that technique cannot be used here because the membranes are crosslinked and would decompose before any glass transition can be observed.

3.4 Hydraulic Permeation through TFCs

The MMCMs should prove adept at rejection large molecular weight solutes, because of the relevant pore sizes of the cage molecules and enhanced robustness from the crosslinking reaction. The solute rejection performance is given in Figure 5; complete molecular weight cut-off curves for each solvent are given in Figure S6. Here we pay greatest attention to the separation factor between the α-methylstyrene dimer and solvent as a more useful metric for comparing membrane selectivity than rejection curves because it amplifies selectivity differences and focuses on the low molecular weight solute range more relevant to most separations of commercial interest. Permeances varied from 0.04 to 5.5 Lm⁻²h⁻¹bar⁻¹ depending on the solvent and the ASPOC loading. Interestingly, permeance was not proportional to solvent size or viscosity. Rather it is correlated closely with the solvent's ability to swell Matrimid.

The importance of polymer swelling was supported by Figure 6, showing the relation between the solvent permeance and the squared difference of the Hansen solubility parameters of Matrimid for each solvent. The observed general downward trend in permeance as the square difference increased regardless of ASPOC loading suggests that the degree of interaction between the polymer backbone and solvent is the primary determinant of relative permeance. Since the crosslinker used in the reaction is a ten-carbon chain, the crosslinked backbones of the main polymer likely have significantly more freedom to increase free volume in high swelling, high-interaction solvents than what is normally observed in more tightly crosslinked polymers. Conversely, there is little driving force in low-interaction solvents to space the chains out, so the membrane system remains in a lower free volume conformation.

If solvent interactions control polymer chain spacing, the separation factors for solvent dimers should be inversely proportional to permeance, with higher separation factors in lower-swelling solvents. However, this is not what we observed. For crosslinked Matrimid, the separation factors decreased in the order methanol > toluene > ethanol > THF > heptane > acetonitrile, and so polymer swelling cannot be the only contributor to separation performance. Among other potentially important factors are dimer (solute) conformation[37]; aromatic vs. aliphatic

interactions among solute, solvent, and polymer[38], solute aggregation, the dynamics of polymer motion, and perhaps occupancy of free volume elements by co-solutes. Better understanding of the interplay between different aspects of intermolecular interactions is vital to understanding membrane transport in the OSN and OSRO transport regimes. As shown in Figure 5 and Figure S6, increasing ASPOC loading provided a monotonic increase in permeance for all solvents, and a consistent increase in the molecular weight cutoff (decrease in small-molecule rejection) of styrene oligomers with some variation among solvents. Thus, only the MMCM containing 2.6% ASPOC gave better rejection of α-methylstyrene dimer than Matrimid in most solvents. The MMCM containing the highest ASPOC loading (9.4 vol%), provided 90% or higher rejection of styrene oligomers beginning at approximately 4-10 units in the polar solvents (MeCN, THF, EtOH, MeOH), but not in toluene or heptane. We have previously demonstrated that ASPOCs can impart mild antiplasticization effects when mixed with polymers, which we believe occurs via a cage-induced reduction in polymer chain mobility.[21] If we extend this concept to high loadings, we may pass a certain threshold where the density of cage molecules in the membrane is so high that it begins to disrupt chain packing and create new non-selective free volume in the membrane.

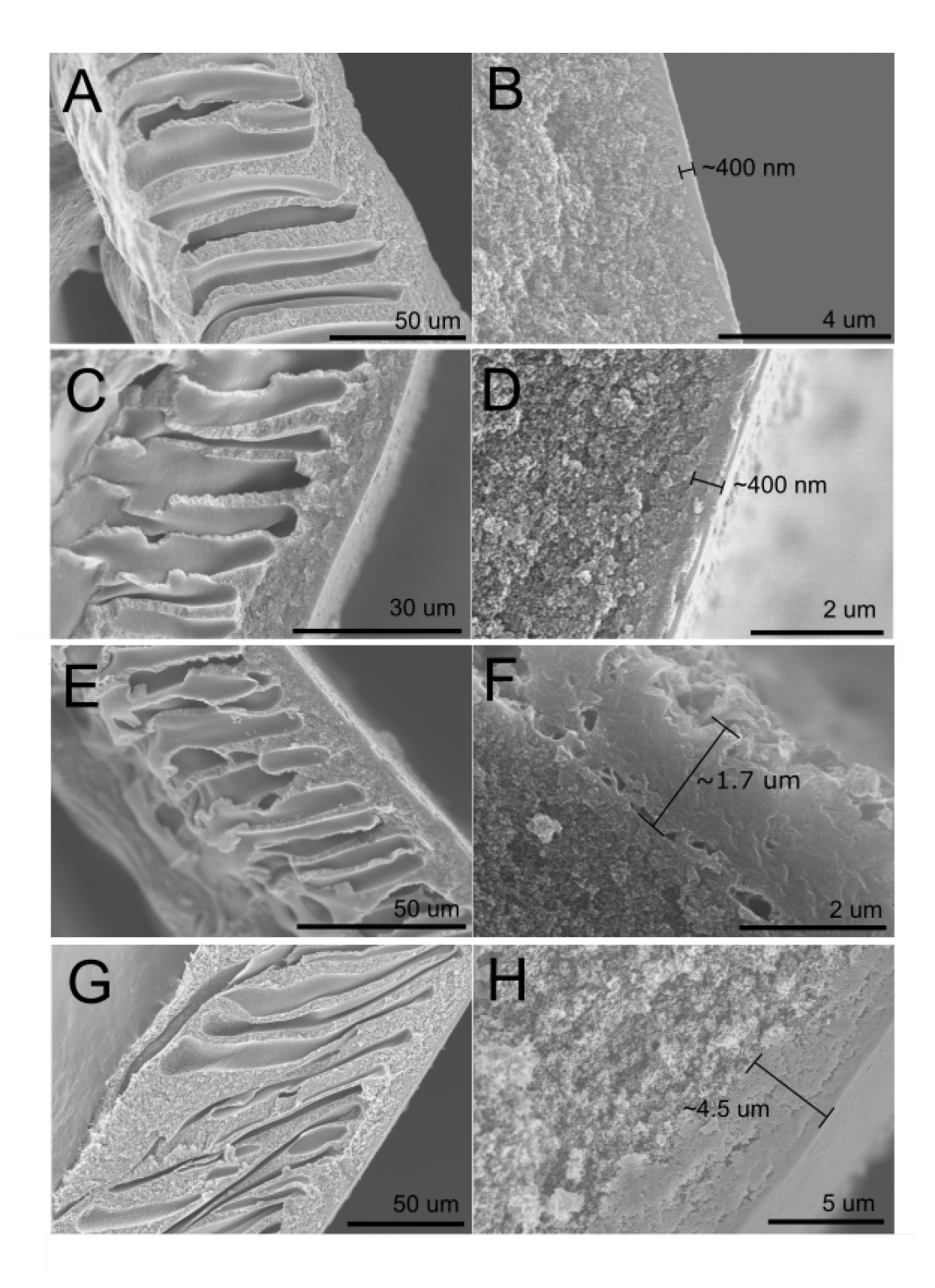


Figure 4: SEM images of TFC membranes after crossflow permeation testing. All samples are crosslinked using the procedure described in Section 2.5. (A)- (B) Matrimid. (C)- (D) 2.6 vol% ASPOC loading MMCM. (E)- (F) 5.7 vol% ASPOC loading MMCM. (G)-(H) 9.4 vol% ASPOC loading MMCM. In (B), (D), (F), (H), bars are placed to indicate the approximate thickness of the topcoat layer.

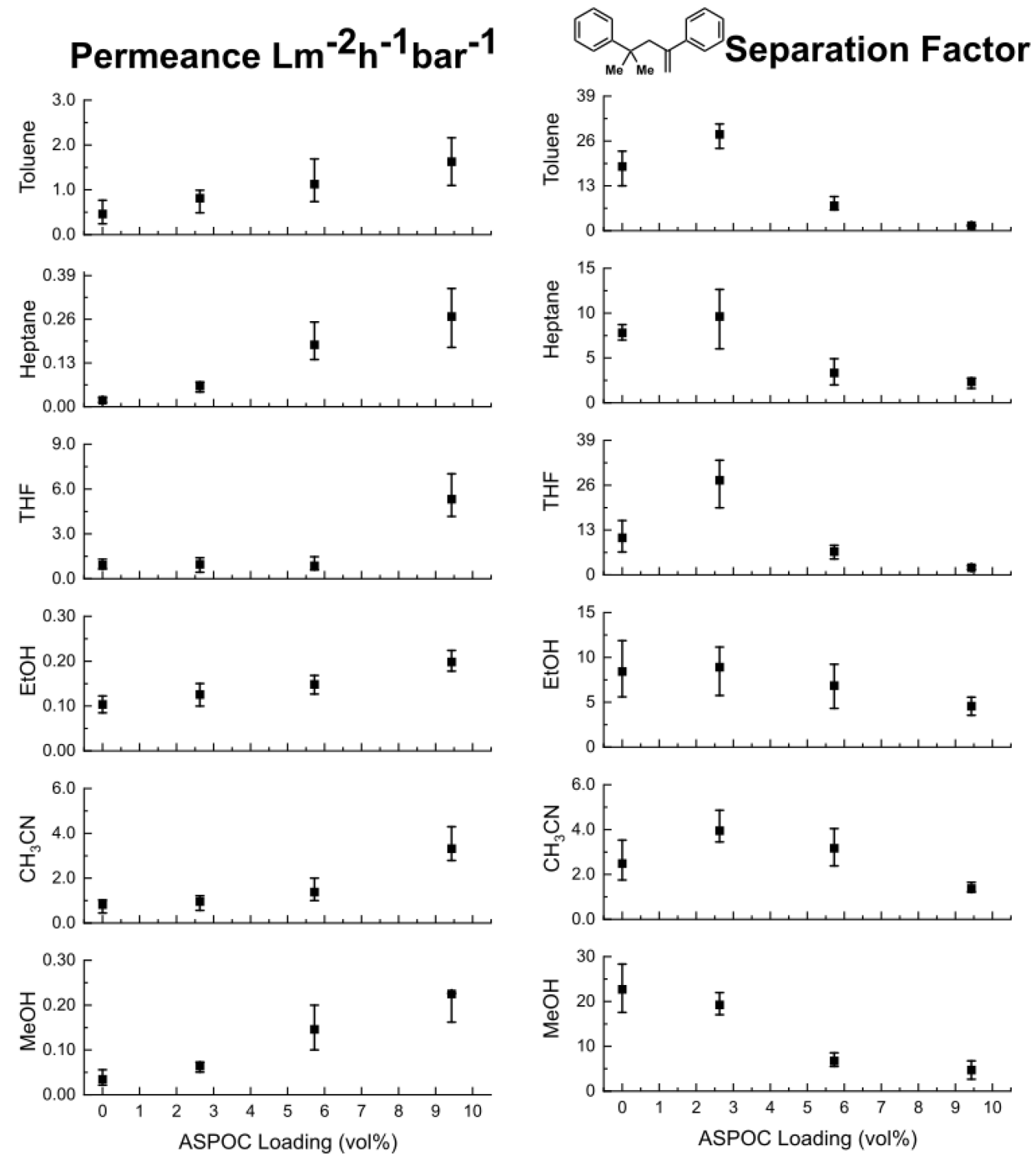


Figure 5: Hydraulic permeance and α-methylstyrene dimer separation factor (i.e., dimer/solvent) of ASPOC MMCM TFCs (N=3). Membranes were tested at 30 bar and 22 $^{\circ}$ C in a crossflow configuration. The feed solution contained 0.05 g/L of α-methylstyrene dimer, and 0.5 g/L each of PS580 and PS1.3k oligomers.

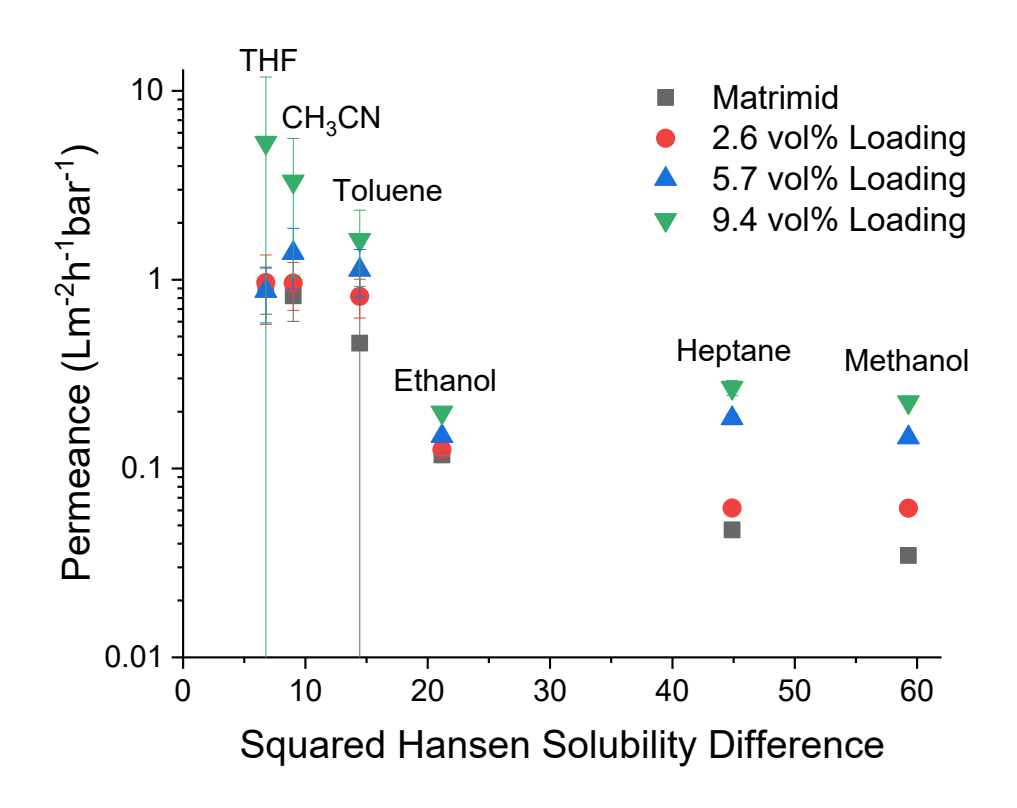


Figure 6: Membrane permeance versus the squared difference in the Hansen solubility parameters between Matrimid and each solvent.

We propose two hypotheses for the nature of the interaction between the polymer and cages at high loading, as illustrated in Figure 7. When the density of ASPOC in the membrane is relatively low (up to approximately 3 vol%), the cages are able to sit in free volume elements or create their own free volume elements by wedging into "Henry sites." The cages are dispersed enough that they do not significantly interact with each other, thus preserving an average interchain distance in the host polymer (designated as d₁ in the figure). As cage loading increases, we suggest that a threshold at which the free volume of the bulk polymer begins to increase is crossed. A similar phenomenon is observed in mechanical nanocomposites, with the performance decline past ~2 vol% loading normally attributed to agglomeration of the filler.[39, 40] In typical nanocomposites, the filler phase is insoluble, but in this work the cages are soluble. This should diminish, but may not entirely eliminate, aggregation of the filler in the MMCM solid solution.

Thus, polymer free volume may increase either by virtue of cage-cage interactions (Fig. 7, left) or cage-polymer interactions (Fig. 7, right). In the former case, aggregates of only a few cages

would be too small to be detected by SEM (Figure 4) but could still have significant effects on membrane performance. Such aggregates would cause localized, nano-scale defects in the area immediately surrounding the aggregate, similar to the sieve-in-a-cage defects commonly encountered in conventional mixed matrix membranes.[41] In contrast, interactions between the cage and polymer may disrupt polymer-polymer interactions, increasing the average chain separation distance to some value d₂, larger than d₁, and thereby increase the free volume throughout the bulk polymer. We cannot distinguish between these hypotheses at present.

It will be important to address these types of issues to make maximum use of molecular cage materials in composite membranes. Presumably, the more selective sieve component(s) we can introduce into a composite membrane, the better its performance will be. It is of course well known that filler and matrix phase properties need to be complementary, both in terms of function and physical interaction, in mixed-matrix membranes.[42] While molecular cage materials like ASPOCs or metal-organic polyhedra are promising in their potential to circumvent some of the compatibility issues seen with traditional MMMs, our results suggest that even these exciting new components have limitations on their ability to boost composite membrane performance.

While the previously discussed experiments involving polystyrene oligomers provided important insight into the micro-scale dynamics that affect solvent transport, we are more interested in the membranes' ability to perform challenging OSRO separations. To test solventsolvent separations, we attempted to separate triisopropylbenzene (TIPB) from toluene in a 95:5 mol% (toluene:TIPB) mixture, with results shown in a Robeson-style plot in Figure 8. We also include additional data gathered previously in our lab to create, to our knowledge, the first multimembrane tradeoff plot for an OSRO-class separation. Consistent with the α-methylstyrene rejection results above, the separation factor for the new materials was largest (9.7) at 2.6 vol% cage loading and decreased to approximately 4 with increased ASPOC loading. Contrary to the polystyrene experiments, however, toluene permeance decreased sharply from 2 Lm⁻²h⁻¹bar⁻¹ to 0.16 Lm⁻²h⁻¹bar⁻¹ upon incorporation of 2.6 vol% ASPOC cage into the crosslinked Matrimid material. Permeance rebounded to 0.4-0.9 Lm⁻²h⁻¹bar⁻¹ with more ASPOC incorporation. We hypothesize that TIPB may partially enter the cage windows without ever being able to fully diffuse through such that the cage becomes inaccessible to toluene. This effect is likely less pronounced in the case of the α -methyl styrene dimer, as the linear conformation of that solute can more easily diffuse out of the cage relative to TIPB. The TIPB-occluded cages act as barriers to

solvent diffusion and thus lower the toluene permeance. At higher loadings, the effect becomes less pronounced, likely due to the bulk free volume increase described above. While no definitive conclusions can be drawn from so few data points, the apparent success of ASPOC incorporation in enhancing both permeance and separation under some conditions augurs well for further exploration of such materials.

We also highlight the positive effects of the crosslinking reaction in Figure 9 where trade-off plots for the separation of the α -methylstyrene dimer (Fig. 9a) and toluene/TIPB (Fig. 9b) are shown. In Fig. 9a, we observe that crosslinking imparts a sharp increase in the dimer separation factor for both Matrimid and the 2.6 vol% loading MMCM and only a slight decline in permeance. This is likely due to a decline in polymer-phase swelling in the crosslinked membranes and corresponding improvement in the separation capabilities as a result. In Fig. 9b, it is notable that only the crosslinked MMCM is able to distinguish between toluene and TIPB to any appreciable degree, albeit at the cost of toluene permeance. We similarly attribute this observation to a combination of the decline in polymer swelling and partial occlusion of the cages by the TIPB molecules. Despite the decline in permeance, we highlight the synergistic effect of crosslinking and inclusion of the cages, which results in the highest separation factor in both systems.

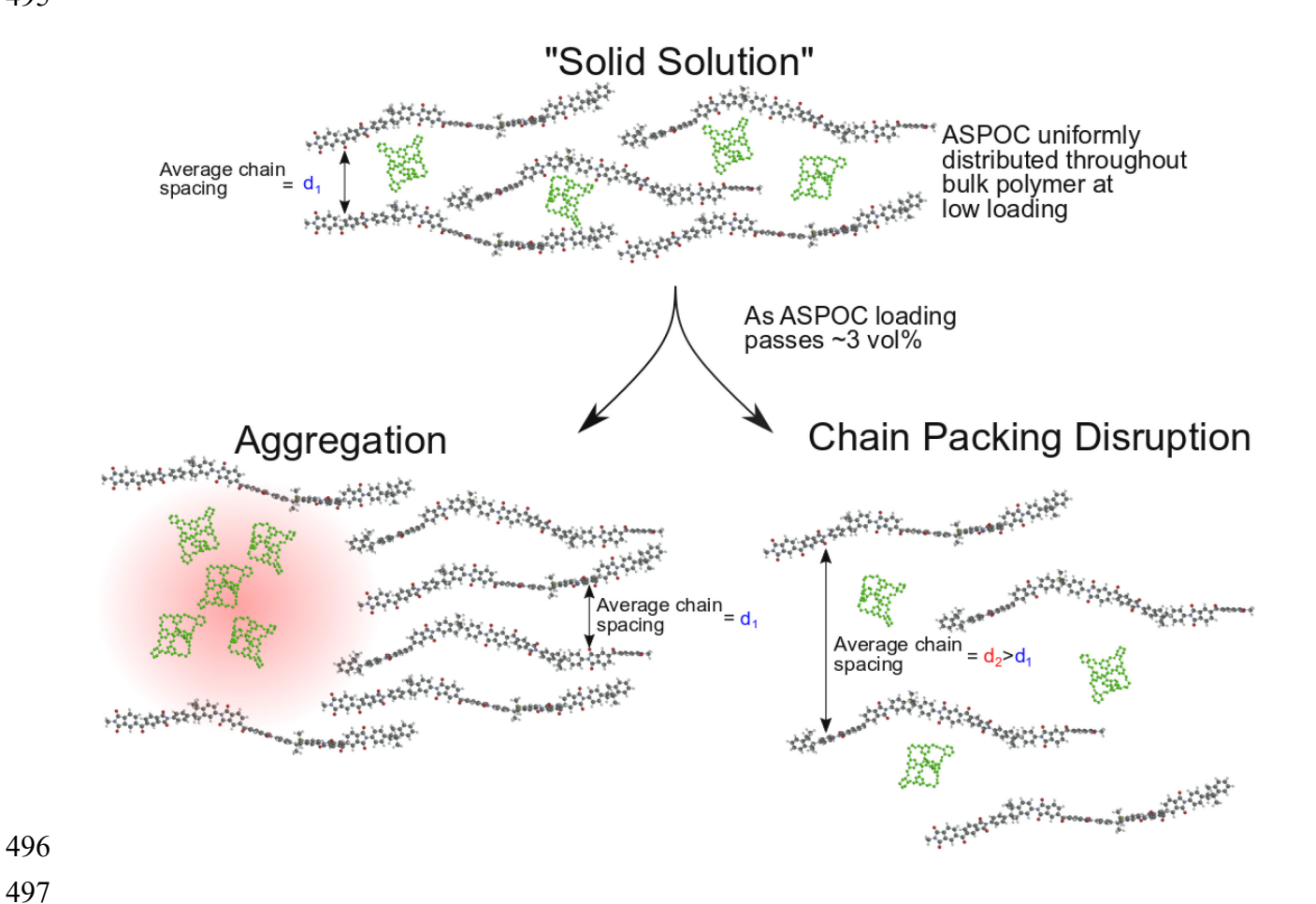


Figure 7: Two hypotheses of the effect of increasing ASPOC loading (shown in green) on membrane microstructure. Lower left: dominant cage-cage interactions in which excess free volume (highlighted in red) is caused by the cage agglomerate. Lower right: dominant cage-polymer interactions in which average interchain distance is increased from d_1 to d_2 due to higher loading of the cages. The relative sizes of the cages and polymer chains are not to scale and crosslinkers have been omitted for clarity.

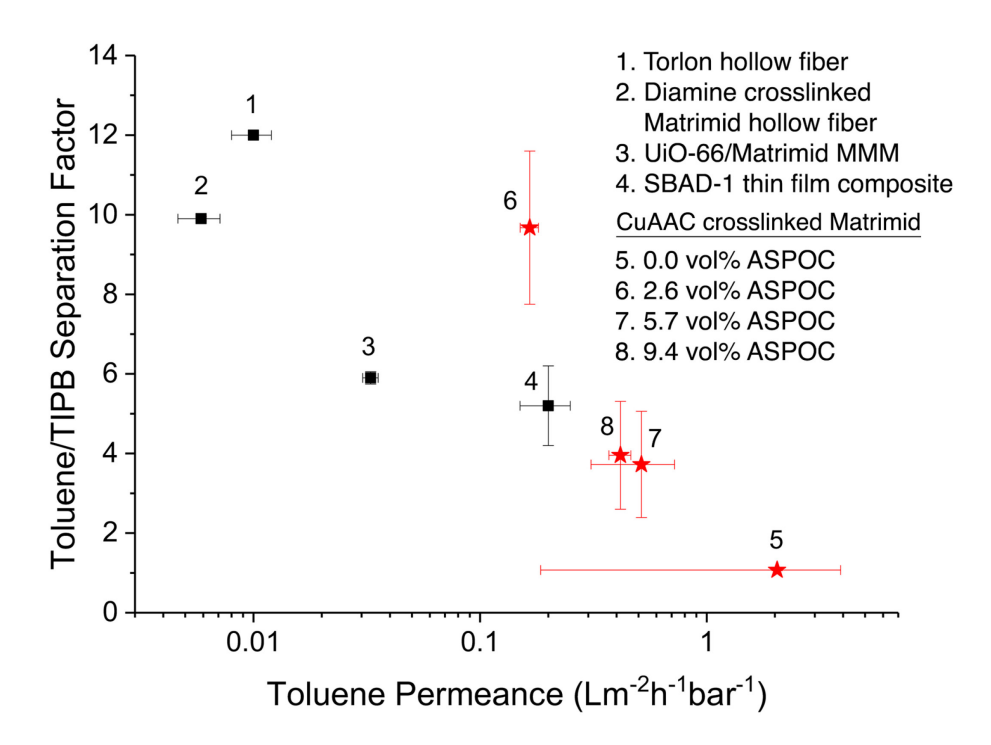


Figure 8: Robeson-style plot of the separation of toluene and triisopropylbenzene by the indicated membranes. Membranes in the present work are labeled as red stars. Points 1 and 4 are from references [43] and [44], respectively.

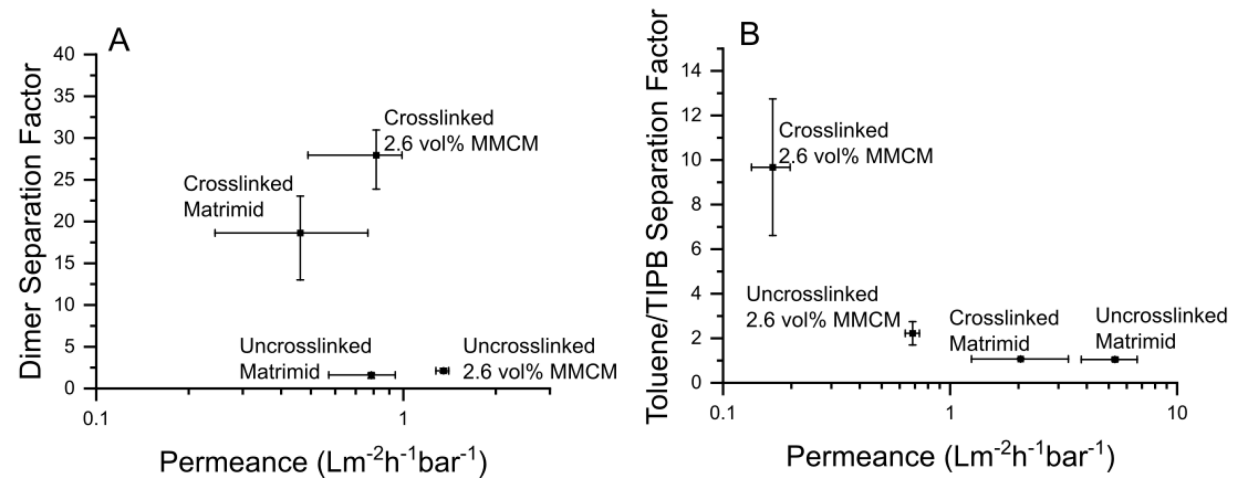


Figure 9: Tradeoff plots comparing the separation performance of crosslinked and uncrosslinked Matrimid and MMCMs with 2.6 vol% cage loading. (A) Separation factor and permeance for the α-methylstyrene dimer from the toluene/polystyrene mixture described previously (B) Separation factor and permeance in the mixture of toluene and triisopropylbenzene described previously.

4. Conclusions

Here, we employed the copper-catalyzed azide-alkyne cycloaddition reaction to crosslink the polyimide Matrimid as a method compatible with the incorporation of "zero-dimensional" amorphous scrambled porous organic cage molecules. The resulting crosslinked molecularly mixed composite membranes were assessed for their ability to reject large solutes via standardized polystyrene oligomers in a variety of organic solvent environments. The ability of the membranes to perform organic solvent reverse osmosis was also investigated using the separation of toluene and triisopropylbenzene as a test case. The ability to perform a solvent-solvent separation suggests that the membranes operate through a chemical potential-driven, OSRO mechanism, although they prove adept at differentiating between larger solutes as well. Surprisingly, the addition of cage molecules beyond a certain threshold was found to be detrimental to membrane selectivity; however, a potential optimum loading was found that resulted in membranes with high separation factors and meaningful solvent permeances. Two hypotheses explaining this phenomenon are presented, both consistent with the data in hand. Thus, as cage loading increases, cage-cage interactions may become significant and cause agglomeration, leading to membrane defects. Alternatively, cage-polymer interactions may become greater than polymer-polymer interactions and disrupt polymer chain packing. Hence, a cage loading is eventually reached where performance improvement from the presence of the cages is offset by decline in polymer-phase selectivity. We acknowledge that the underlying mass transport processes in these membranes is not well understood, but plan to investigate this topic further in future work. Using data from our lab, we have also made a Robeson-style tradeoff plot for the separation of toluene and triisopropylbenzene and shown preliminary support for the ability of MMCMs to surpass traditional polymer performance limitations. It will be essential to gain a greater fundamental understanding of the nature of the interactions between polymers and zero-dimensional cage materials in the future. The current work presents significant preliminary findings necessary to develop fundamental insight for MMCMs and underscores their ease of fabrication and their ability to perform challenging solvent-solvent separations.

542

543

544

545

546

516

517

518

519

520

521

522

523

524

525

526

527

528

529

530

531

532

533

534

535

536

537

538

539

540

541

Acknowledgements

The authors thank the National Science Foundation (CBET 1653153) for funding this research.

Notes

The authors declare no competing financial interest.

- 549 References
- 550 [1] W.J. Koros, R.P. Lively, Water and beyond: Expanding the spectrum of large-scale energy
- efficient separation processes, AIChE Journal, 58 (2012) 2624-2633.
- 552 [2] R.W. Baker, K. Lokhandwala, Natural Gas Processing with Membranes: An Overview,
- Industrial & Engineering Chemistry Research, 47 (2008) 2109-2121.
- [3] W.J. Koros, R. Mahajan, Pushing the limits on possibilities for large scale gas separation: which
- strategies?, Journal of Membrane Science, 175 (2000) 181-196.
- 556 [4] B.-H. Jeong, E.M.V. Hoek, Y. Yan, A. Subramani, X. Huang, G. Hurwitz, A.K. Ghosh, A.
- Jawor, Interfacial polymerization of thin film nanocomposites: A new concept for reverse osmosis
- membranes, Journal of Membrane Science, 294 (2007) 1-7.
- 559 [5] D.R. Paul, J.D. Paciotti, Driving force for hydraulic and pervaporative transport in
- homogeneous membranes, Journal of Polymer Science: Polymer Physics Edition, 13 (1975) 1201-
- 561 1214.
- [6] L.M. Robeson, The upper bound revisited, Journal of Membrane Science, 320 (2008) 390-400.
- [7] N. Kosinov, J. Gascon, F. Kapteijn, E.J.M. Hensen, Recent developments in zeolite membranes
- for gas separation, Journal of Membrane Science, 499 (2016) 65-79.
- [8] T.G. Grissom, C.H. Sharp, P.M. Usov, D. Troya, A.J. Morris, J.R. Morris, Benzene, Toluene,
- and Xylene Transport through UiO-66: Diffusion Rates, Energetics, and the Role of Hydrogen
- Bonding, The Journal of Physical Chemistry C, 122 (2018) 16060-16069.
- 568 [9] C. Zhang, R.P. Lively, K. Zhang, J.R. Johnson, O. Karvan, W.J. Koros, Unexpected Molecular
- 569 Sieving Properties of Zeolitic Imidazolate Framework-8, The Journal of Physical Chemistry
- 570 Letters, 3 (2012) 2130-2134.
- 571 [10] C. Zhang, K. Zhang, L. Xu, Y. Labreche, B. Kraftschik, W.J. Koros, Highly scalable ZIF-
- 572 based mixed-matrix hollow fiber membranes for advanced hydrocarbon separations, AIChE
- 573 Journal, 60 (2014) 2625-2635.

- 574 [11] G. Liu, V. Chernikova, Y. Liu, K. Zhang, Y. Belmabkhout, O. Shekhah, C. Zhang, S. Yi, M.
- 575 Eddaoudi, W.J. Koros, Mixed matrix formulations with MOF molecular sieving for key energy-
- 576 intensive separations, Nat Mater, 17 (2018) 283-289.
- 577 [12] S. Husain, W.J. Koros, Mixed matrix hollow fiber membranes made with modified HSSZ-13
- zeolite in polyetherimide polymer matrix for gas separation, Journal of Membrane Science, 288
- 579 (2007) 195-207.
- 580 [13] Z.V. Singh, L.-L. Tan, M.G. Cowan, Y.-W. Yang, W. Zhang, D.L. Gin, R.D. Noble,
- Pillar [5] arene/MatrimidTM materials for high-performance methane purification membranes,
- 582 Journal of Membrane Science, 539 (2017) 224-228.
- 583 [14] C. Zhang, W.J. Koros, Ultraselective Carbon Molecular Sieve Membranes with Tailored
- 584 Synergistic Sorption Selective Properties, Adv Mater, 29 (2017).
- 585 [15] T. Tozawa, J.T. Jones, S.I. Swamy, S. Jiang, D.J. Adams, S. Shakespeare, R. Clowes, D.
- 586 Bradshaw, T. Hasell, S.Y. Chong, C. Tang, S. Thompson, J. Parker, A. Trewin, J. Bacsa, A.M.
- 587 Slawin, A. Steiner, A.I. Cooper, Porous organic cages, Nat Mater, 8 (2009) 973-978.
- 588 [16] D.B. Shinde, G. Sheng, X. Li, M. Ostwal, A.-H. Emwas, K.-W. Huang, Z. Lai, Crystalline
- 589 2D Covalent Organic Framework Membranes for High-Flux Organic Solvent Nanofiltration,
- Journal of the American Chemical Society, 140 (2018) 14342–14349.
- 591 [17] Y. Cheng, Y. Ying, S. Japip, S.D. Jiang, T.S. Chung, S. Zhang, D. Zhao, Advanced Porous
- Materials in Mixed Matrix Membranes, Adv Mater, (2018) e1802401.
- 593 [18] J.D. Evans, D.M. Huang, M.R. Hill, C.J. Sumby, A.W. Thornton, C.J. Doonan, Feasibility of
- 594 Mixed Matrix Membrane Gas Separations Employing Porous Organic Cages, The Journal of
- 595 Physical Chemistry C, 118 (2014) 1523-1529.
- 596 [19] Y. Jin, B.A. Voss, R.D. Noble, W. Zhang, A Shape-Persistent Organic Molecular Cage with
- 597 High Selectivity for the Adsorption of CO2 over N2, Angewandte Chemie International Edition,
- 598 49 (2010) 6348-6351.

- 599 [20] Y. Jin, B.A. Voss, A. Jin, H. Long, R.D. Noble, W. Zhang, Highly CO2-Selective Organic
- 600 Molecular Cages: What Determines the CO2 Selectivity, Journal of the American Chemical
- 601 Society, 133 (2011) 6650-6658.
- 602 [21] G. Zhu, F. Zhang, M.P. Rivera, X. Hu, G. Zhang, C.W. Jones, R.P. Lively, Molecularly Mixed
- 603 Composite Membranes for Advanced Separation Processes, Angewandte Chemie International
- 604 Edition, 58 (2019) 2638-2643.
- 605 [22] Q. Song, S. Jiang, T. Hasell, M. Liu, S. Sun, A.K. Cheetham, E. Sivaniah, A.I. Cooper, Porous
- 606 Organic Cage Thin Films and Molecular-Sieving Membranes, Advanced Materials, 28 (2016)
- 607 2629-2637.
- 608 [23] G. Zhu, Y. Liu, L. Flores, Z.R. Lee, C.W. Jones, D.A. Dixon, D.S. Sholl, R.P. Lively,
- 609 Formation Mechanisms and Defect Engineering of Imine-Based Porous Organic Cages, Chemistry
- 610 of Materials, 30 (2017) 262-272.
- 611 [24] S. Jiang, J.T.A. Jones, T. Hasell, C.E. Blythe, D.J. Adams, A. Trewin, A.I. Cooper, Porous
- organic molecular solids by dynamic covalent scrambling, Nature Communications, 2 (2011) 207.
- 613 [25] G. Zhu, D. O'Nolan, R.P. Lively, Molecularly Mixed Composite Membranes: Challenges and
- Opportunities, Chemistry A European Journal, 26 (2020) 3464-3473.
- 615 [26] R. Wijiyanti, A.N. Ubaidillah, T. Gunawan, Z.A. Karim, A.F. Ismail, S. Smart, R. Lin, N.
- Widiastuti, Polysulfone mixed matrix hollow fiber membranes using zeolite templated carbon as
- a performance enhancement filler for gas separation, Chemical Engineering Research and Design,
- 618 (2019).
- 619 [27] R. Mahajan, R. Burns, M. Schaeffer, W.J. Koros, Challenges in forming successful mixed
- 620 matrix membranes with rigid polymeric materials, Journal of Applied Polymer Science, 86 (2002)
- 621 881-890.
- 622 [28] A.M. Marti, S.R. Venna, E.A. Roth, J.T. Culp, D.P. Hopkinson, Simple Fabrication Method
- 623 for Mixed Matrix Membranes with in Situ MOF Growth for Gas Separation, ACS Appl Mater
- 624 Interfaces, 10 (2018) 24784-24790.

- 625 [29] Q. Qian, A. Wu, W.S. Chi, P.A. Asinger, S. Lin, A.J. Hypsher, Z.P. Smith, Mixed-matrix
- 626 membranes formed from imide-functionalized UiO-66-NH2 for improved interfacial
- 627 compatibility, ACS Applied Materials & Interfaces, (2019).
- 628 [30] J.D. Wind, C. Staudt-Bickel, D.R. Paul, W.J. Koros, The Effects of Crosslinking Chemistry
- on CO2 Plasticization of Polyimide Gas Separation Membranes, Industrial & Engineering
- 630 Chemistry Research, 41 (2002) 6139-6148.
- [31] R.A. Evans, The Rise of AzideAlkyne 1,3-Dipolar Click Cycloaddition and its Application to
- Polymer Science and Surface Modification, Aust. J. Chem., 60 (2007) 384-395.
- [32] N. Naga, H. Nagino, H. Furukawa, Synthesis of organic-inorganic hybrid gels by means of
- thiol-ene and azide-alkene reactions, Journal of Polymer Science Part A: Polymer Chemistry, 54
- 635 (2016) 2229-2238.
- 636 [33] Z. Gonda, Z. Novák, Highly active copper-catalysts for azide-alkyne cycloaddition, Dalton
- 637 Transactions, 39 (2010) 726-729.
- 638 [34] Z. Zhai, C. Jiang, N. Zhao, W. Dong, P. Li, H. Sun, Q.J. Niu, Polyarylate membrane
- 639 constructed from porous organic cage for high-performance organic solvent nanofiltration, Journal
- 640 of Membrane Science, 595 (2020) 117505.
- [35] A. Carné-Sánchez, G.A. Craig, P. Larpent, T. Hirose, M. Higuchi, S. Kitagawa, K. Matsuda,
- 642 K. Urayama, S. Furukawa, Self-assembly of metal-organic polyhedra into supramolecular
- polymers with intrinsic microporosity, Nature Communications, 9 (2018) 2506.
- [36] F. Gimblett, A. Rahman, K. Sing, The origin of porosity in hydrous zirconia gels. II. Mixed
- microporous/mesoporous gels, Journal of colloid and interface science, 102 (1984) 483-490.
- 646 [37] Y. Liu, Z. Chen, G. Liu, Y. Belmabkhout, K. Adil, M. Eddaoudi, W. Koros, Conformation-
- 647 Controlled Molecular Sieving Effects for Membrane-Based Propylene/Propane Separation,
- 648 Advanced Materials, 0 (2019) 1807513.
- [38] S.R. Hosseinabadi, K. Wyns, V. Meynen, A. Buekenhoudt, B. Van der Bruggen, Solvent-
- 650 membrane-solute interactions in organic solvent nanofiltration (OSN) for Grignard functionalised

- ceramic membranes: Explanation via Spiegler-Kedem theory, Journal of Membrane Science, 513
- 652 (2016) 177-185.
- 653 [39] J.-H. Chang, Y.U. An, Nanocomposites of polyurethane with various organoclays:
- Thermomechanical properties, morphology, and gas permeability*, Journal of Polymer Science
- 655 Part B: Polymer Physics, 40 (2002) 670-677.
- 656 [40] M.Z. Rong, M.Q. Zhang, Y.X. Zheng, H.M. Zeng, R. Walter, K. Friedrich, Structure-property
- 657 relationships of irradiation grafted nano-inorganic particle filled polypropylene composites,
- 658 Polymer, 42 (2001) 167-183.
- 659 [41] R. Mahajan, W.J. Koros, Factors Controlling Successful Formation of Mixed-Matrix Gas
- Separation Materials, Industrial & Engineering Chemistry Research, 39 (2000) 2692-2696.
- [42] T.T. Moore, W.J. Koros, Non-ideal effects in organic—inorganic materials for gas separation
- membranes, Journal of Molecular Structure, 739 (2005) 87-98.
- 663 [43] H.-Y. Jang, J.R. Johnson, Y. Ma, R. Mathias, D.A. Bhandari, R.P. Lively, Torlon® hollow
- 664 fiber membranes for organic solvent reverse osmosis separation of complex aromatic hydrocarbon
- 665 mixtures, AIChE Journal, 65 (2019) e16757.
- 666 [44] K.A. Thompson, R. Mathias, D. Kim, J. Kim, N. Rangnekar, J.R. Johnson, S.J. Hoy, I. Bechis,
- A. Tarzia, K.E. Jelfs, B.A. McCool, A.G. Livingston, R.P. Lively, M.G. Finn, N-
- Aryl-linked spirocyclic polymers for membrane separations of complex hydrocarbon mixtures,
- 669 Science, 369 (2020) 310-315.